XXIV Biennial Symposium on Measuring Techniques in Turbomachinery
Prague, Czech Republic, 29 - 31 August 2018
Paper No MTT2418B42

EXPERIMENTAL AND NUMERICAL INVESTIGATION OF THE BOUNDARY LAYER TRANSITION ON THE PRISMATIC BLADE

E. Flídr, T. Jelínek, P. Straka
Czech Aerospace Research Centre, Prague,
Czech Republic

Keywords: boundary layer transition, turbine cascade, infrared thermography

ABSTRACT

The contribution describes experimental and numerical investigation of the laminar-turbulent boundary layer transition on a prismatic blade in a linear blade cascade. Experiments were performed using infrared thermography (IRT), while numerical simulations were based on the different transition models implemented into the in-house numerical codes. Both approaches are then compared.

NOMENCLATURE

Symbol	Name	Dimension
c	Blade pitch	m
c_f	Skin friction coefficient	1
E	Emissive power	W/m^2
h	Heat transfer coefficient	$W/(m^2K)$
l	Characteristic length	m
R	Radiation reflection	W
t	Blade chord	m
T	Thermodynamic temperature	K
u	Velocity	m/s
Nu	Nusselt number	1
Re	Reynolds number	1
ε	Emissivity	1
η	Spectral range	nm
λ	Thermal conductivity	W/(mK)
ν	Kinematic viscosity	m^2/s
σ	Stefan-Boltzmann constant	W/m^2K^4
φ	Surface curvature	m^{-1}

INTRODUCTION

Kinetic energy is dissipated due to the viscous forces that are connected with the presence of the turbine blades in the flow field. This energy dissipation is strongly dependent on the boundary layer (BL) character on the blade surface and also on the BL separation in subsonic flow. Intensive experimental and numerical research is being carried out because of dependency between turbine efficiency and energy dissipation of the flow.

BL transition is commonly described by similarity criteria such as Mach and Reynolds numbers, which describe effects of compressibility and viscous forces. BL transitions is also influenced by free stream turbulence and pressure gradients, see e.g. Narasimha [1] or Mayle [2].

Many experimental techniques can be used for the detection of BL transition. Hot-film anemometry (HFA) (Gomes et al. [3]), pressure sensitive paint (Balla [4]) or oil flow visualization (Cattafesta et al. [5]), can be mentioned. Infrared thermography (IRT) is also commonly used for the detection of the BL transition, see e.g. [6]. Principle of this method is based on different convective heat transfer in laminar and turbulent flow. The laminar BL can be considered as an insulator due to its low heat exchange between the model surface and free stream.

Key elements for obtaining the meaningful experimental results are:

- Different temperatures between the model surface and free stream (some kind of heating or cooling of the models are often used, see e.g. [7]).
- Low thermal conductivity of material used for model manufacturing.

EXPERIMENTAL APPARATUS, METHODS AND SETUP

Wind tunnel

Experiments were performed in the low-pressure closed loop wind tunnel (WT). Scheme of the WT is shown in Figure 1. Mach number can be set by changing the rotational speed of the compressor, while the change of the Reynolds number can be achieved by reduction of the pressure in the WT by set of vacuum pumps, so each of these numbers can be set separately. Incidence angle of the flow can be adjusted using pair of shaped semi-nozzles placed in front of the fixed blade cascade. Incidence angle was set at $\alpha = 85°$ in presented experiments, see Figure 2.

Linear blade cascade was ensembled of 9 blades that were placed between two walls of the WT test section. Pitch-to-chord ratio of the cascade was $t/c = 0.9$. For the presented experiments one blade in the cascade was manufactured of CibaTool® (artificial wood). As was mentioned

above thanks to the low thermal conductivity of this material the blade could have been used for detection of the BL transition using IRT.

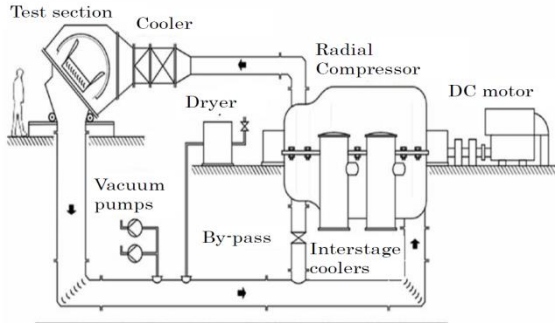

Figure 1: Scheme of the wind tunnel.

Infrared thermography

Principle of IRT is based on measurement of thermal radiation of the body under investigation. Relation between the temperature and surface emissive power is described by well-known Stefan-Boltzmann law:

$$E = \varepsilon\sigma T^4, \qquad (1)$$

where ε is the emissivity of the body (for black body $\varepsilon = 1$), $\sigma = 5.68\times10^{-8}$ W/m^{2}K^4 is Stefan-Boltzmann constant and T is thermodynamic temperature. Camera must be carefully calibrated for an accurate temperature measurement. Emissivity of the body ε is dependent on many variables[1]. In this case ε was mainly function of:

$$\varepsilon = f(T, \varphi, R), \qquad (2)$$

where φ is the direction of radiation and R is the reflection of the radiation from the body.

Main advantage of this method compared to others (e.g. hot-films) in the fluid dynamics investigation is, that camera does not influence the flow field, and also whole 2D temperature field can be measured. Disadvantage is that many parameters can influence temperature measurement and already mentioned calibration with high precision must be performed before measurement.

Infrared camera setup

FLIR A655sc infrared camera with resolution of 640 × 480 pixels and maximum frame rate of 50 Hz was used for the experiments. View angle of the camera was 15°. Camera can clearly detect 30 × 10^{-3}°C differences in temperature. Spectral range of the camera is η = 7.5 ÷ 14 μm. Standard temperature range for the FLIR A655sc is T = (-40 ÷ 150) °C and it can operate in the temperature range of T = (-10 ÷ 50) °C. Best accuracy of the camera is ± 2 °C or ± 2% rdg. The original calibration made by producer was used during the experiments..

[1] Another variable can be roughness of the surface, spectral range η …

Camera was placed 260 mm behind the trailing edges of the blades. Two blades were in the view angle of the camera as can be seen in Figure 2. From the figure it is also obvious, that because of the cascade geometry IR camera could not measure temperature on the leading edge of the blade. Temperature was measured by the IR camera in the range of $s/s_{max} \in (0.2 – 1.0)$.

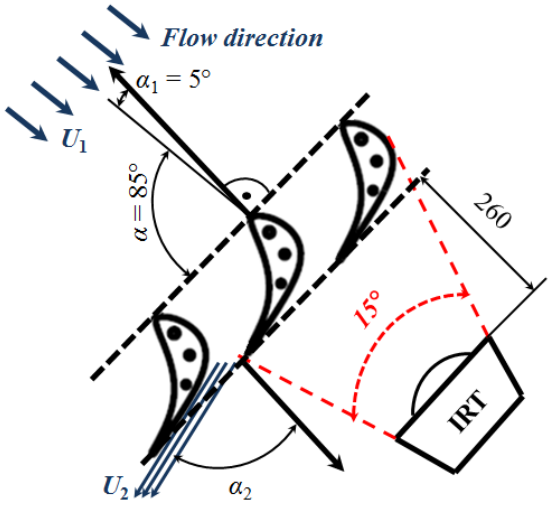

Figure 2: Blade cascade with IR camera.

Detection of the boundary layer transition

As was mentioned above, heat transfer between the free stream and the body surface is dependent on the BL type on its surface, on its thickness δ and also on BL separation, if occurs. This is caused by the increase of skin friction coefficient $c_f = \tau_w/(2\rho u^2)$, that is usually one order higher in turbulent BL compared to laminar one. According to Reynolds analogy, heat transfer is a function of skin friction coefficient in the form:

$$\mathrm{Nu} = \tfrac{1}{2}\, c_f(x)\, \mathrm{Re}, \qquad (3)$$

where Nu = hl/λ is Nusselt number (h is the heat transfer coefficient, l is the characteristic length and λ is the thermal conductivity), Re = ul/ν is Reynolds number (u is the flow velocity and ν is the kinematic viscosity). Air was used as a medium for the experiments, so the Prandtl number was approximately 1 and the condition for Reynolds analogy was satisfied.

Experimental setup

During the experiments several flow regimes defined by outlet isentropic Mach (M_{2is}) and Reynolds (Re_{2is}) numbers were investigated. Regimes were chosen with respect to the WT operation conditions and also with respect to the earlier experiments performed in our laboratory, where the transition of the BL was proven by HFA, see [15], [16]. All tested regimes are summarized in Table 1, where temperatures of the free stream (T_a) and blade temperature (T_{sref}) are also listed. As

can be seen the free stream temperature was higher compare to blade surface (approximately about 1°C) and so the blade was heated by the oncoming flow during the experiments. Blade was not forced heated nor cooled by any external source. Experiments performed with heated blade were already published in [15].

Table 1: Tested flow regime.

M_{2is} [1]	Re_{2is} [1]	T_{sref} [°C]	T_a [°C]
0.8	5.0×10^5	12.7	14.1
0.6	7.5×10^5	12.7	13.5
0.6	5.0×10^5	13.2	14.0
0.6	2.5×10^5	13.1	14.0
0.4	5.0×10^5	12.7	13.3
0.4	2.5×10^5	16.1	16.5

The pressure distribution on the blade surface was measured during the previous experiments. Thirteen pressure taps were equally distributed on the pressure and suction side of the blade.

NUMERICAL APPROACH

Flow in linear blade cascade is modeled as compressible viscous turbulent flow of the perfect gas. Model is described by system of Favre averaged Navier-Stokes equation:

$$\frac{\partial \rho}{\partial t} + \nabla(\rho \mathbf{U}) = 0, \tag{4}$$

$$\frac{\partial (\rho \mathbf{U})}{\partial t} + \nabla(\rho \mathbf{U} \otimes \mathbf{U}) + \nabla p = \nabla \tau, \tag{5}$$

$$\frac{\partial (\rho E)}{\partial t} + \nabla[(\rho E + p)\mathbf{U}] = \nabla(\tau \mathbf{U}) + \nabla(\lambda \nabla T), \tag{6}$$

where ρ is the density, $\mathbf{U}$ is the velocity vector, p is the pressure, τ is the stress tensor, E is the specific total energy, λ is the thermal conductivity and T is the temperature. The system is closed by the equation of state for the perfect gas $p / \rho = r\,T$ and constant specific heat capacity c_p and by two equation nonlinear EARSM k–ω turbulence model of Hellsten [17]:

$$\frac{D(\rho k)}{Dt} = \gamma(P_k - D_k) + \frac{\partial}{\partial x_j}\left[(\mu + \sigma_k \mu_t)\frac{\partial k}{\partial x_j}\right], \tag{7}$$

$$\frac{D(\rho \omega)}{Dt} = P_\omega - D_\omega + \frac{\partial}{\partial x_j}\left[(\mu + \sigma_\omega \mu_t)\frac{\partial \omega}{\partial x_j}\right] + C_D, \tag{8}$$

where k is the turbulent energy, ω is the specific dissipation rate of the turbulent energy, P_k and P_ω are the production terms, D_k and D_ω are the destruction terms, C_D is the cross-diffusion term, μ is the molecular viscosity, μ_t is the turbulent viscosity and σ_k and σ_ω are the model constants. In eq. (7) γ is the intermittency coefficient which will be discussed later.

The in-house numerical code [18] based on the finite volumes method is used for the solution of the system of governing equations (4) – (8).

Boundary layer transition modelling

Two different algebraic models of the BL transition are used in this work. The first model of Straka and Příhoda [19] is based on Narasimhas algebraic relation [1] for the intermittency coefficient:

$$\gamma = 1 - \exp\left[-n\sigma\,(\mathrm{Re_s} - \mathrm{Re_{st}})^2\right], \tag{9}$$

where Re_s is the Reynolds number based on free-stream velocity and on the surface distance from the leading edge, $Re_{st} = f_1(U,\ Tu,\ \theta,\ \lambda)$ is the transition onset criterion depending on the free-stream velocity U, on the free-stream turbulence intensity Tu, on the momentum BL thickness θ and on the pressure gradient λ. Parameters $-n\sigma = f_2(U,\ Tu,\ \theta, \lambda)$ describe turbulent spots generation rate and spots propagation and depend also on the free-stream velocity and turbulence intensity, on the momentum thickness of the BL and on the pressure gradient. Correlations $f_1(U,\ Tu,\ \theta,\ \lambda)$ and $f_2(U,\ Tu,\ \theta,\ \lambda)$ were proposed for both bypass and separation-induced transition mechanism (see [19]).

The intermittency coefficient γ is used in equation (7) for modification of the turbulent energy production and destruction terms and in equations (5) and (6) for evaluation of the effective viscosity $\mu_{eff} = \mu + \gamma \mu_t$.

This transition model is nonlocal because it needs to integrate the boundary layer, to measure the surface distance from the leading edge and to evaluate the free-stream parameters. Therefore, this model is suitable for simple geometries only. In this work it is used for simulation of 2D flow in linear blade cascade.

Very interesting area for modelling of the BL transition is the peripheral part of the blade span near the sidewall due to presence of the secondary vortices. Because above mentioned nonlocal transition model is unusable in this case second model, strictly local formulated, proposed by Kubacki and Dick [20] is used in this work for simulation of 3D flow with an influence of the sidewall.

Model of Kubacki and Dick [20] is also algebraic (it does not need additional transport equation) and is based partially on concept of the intermittency coefficient γ and partially on concept of splitting the turbulent energy k (introduced by Walters and Cokljat [21]) into laminar-fluctuation kinetic energy k_l and the small-scale part k_s as follows: $k_s = f_{ss} \cdot k$, $k_l = k - k_s$, where f_{ss} is the splitting factor. The algebraic transition model of Kubacki and Dick [20] is applied on the production term in transport equation for the turbulent kinetic energy only:

$$\frac{D(\rho k)}{Dt} = \tilde{P}_k - D_k + \frac{\partial}{\partial x_j}\left[(\mu + \sigma_k \mu_t)\frac{\partial k}{\partial x_j}\right], \qquad (10)$$

where $\tilde{P}_k = \gamma P_k + (1-\gamma)P_{sep}$. The first difference from eq. (7) is that only the small-scale component of the turbulent kinetic energy k_s is used for evaluation of the production term P_k. The second difference is the addition of the production term P_{sep} to start the turbulence production due to instability and breakdown of laminar free shear layer.

RESULTS AND DISCUSSION

Determination of the blade emissivity, effects which influence the IRT measurement

Emissivity of the blade under investigation was set according to preparatory experiment. Moreover this experiment was also used for a demonstration of some effects that influence the temperature measurement with IR camera.

For this purpose first part of the blade surface was cleared and served as a reference surface for the blade emissivity determination (right side of the blade in Figure 3). Roughness surface effect on the temperature measurement with IRT was demonstrated by sand paper (middle part of Figure 3) and emissivity together with radiation reflection effect on temperature measurement was demonstrated by aluminum foil (left part of Figure 3).

Reference temperature in the laboratory was measured at steady condition by thermocouple and was $T = 22$ °C. According to this reference temperature, emissivity of the blade surface in the IR camera control software was set as $\varepsilon = 0.93$.

Surface roughness caused that measured temperature was approximately 1°C lower compared to the reference part of the blade; see middle part of Figure 3. Temperature measured on the aluminum foil, which emissivity was $\varepsilon \approx 0.03$, was about 5 °C lower compared to the uncovered surface. Reflection of the radiation on the aluminum foil can be clearly seen. Here reflection from the finger was captured by the IR camera in the left part of Figure 3.

Near the leading edge of the blade ($s/s_{max} \approx 0.2$), effect of the surface curvature was observed as a decrease in the measured temperature. According to Carlomagno and Cardone [22], curvature of the surface starts play important role, when the direction between the radiation and IR camera is higher than 60°, it can be seen on both Figures 3 and 4 at the coordinate ($s/s_{max} \approx 0.2$).

Wind tunnel testing

Picture without the air flow, when the tunnel was turned off, is shown in Figure 4. In the figure reflection from both sidewalls of the WT test section can be seen. Near the leading edge ($s/s_{max} \approx 0.2$) of the blade was a region, where the reflected radiation from another blade in the cascade can be recognized. Surface curvature effect described above, was also observed here.

Visualization of the BL transition is shown in Figure 5. Transition of the BL can be observed as a large temperature gradient on the blade surface.

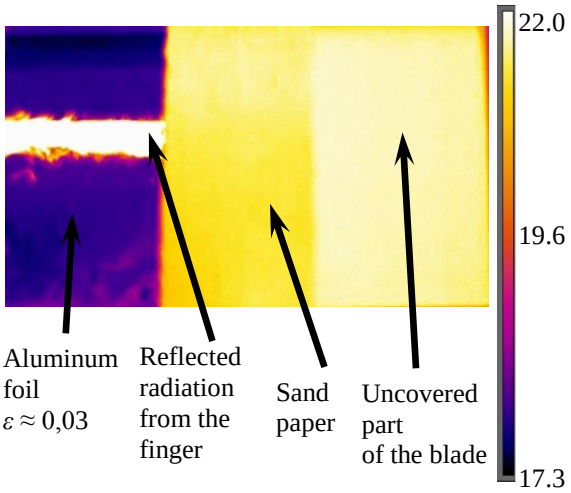

Figure 3: Visualization of the effects influencing the temperature measurement using IRT (scale in the figure is in °C).

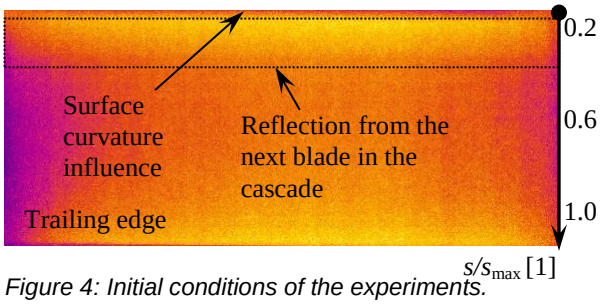

Figure 4: Initial conditions of the experiments.

Effect of Reynolds number can be observed in Figure 5. The highest Reynolds number was $Re_{2is} = 7.5 \times 10^5$ (Figure 5 b), where the BL transition occurred in the $s/s_{max} = 0.6$. With decreasing Reynolds number (Figures 5b and c) position of the BL transition moved downstream toward the trailing edge of the blade. Positions of the BL transition were then $s/s_{max} = 0.7$ for $Re_{2is} = 5.0 \times 10^5$ and $s/s_{max} = 0.8$ for $Re_{2is} = 2.5 \times 10^5$, respectively. The effect of Mach number is visible by comparison of Figure 5 a, c and e and Figure 5d and f. It shows that the effect of Mach number on the position of the BL transition was not significant, because position of the BL transition did not change with Mach number.

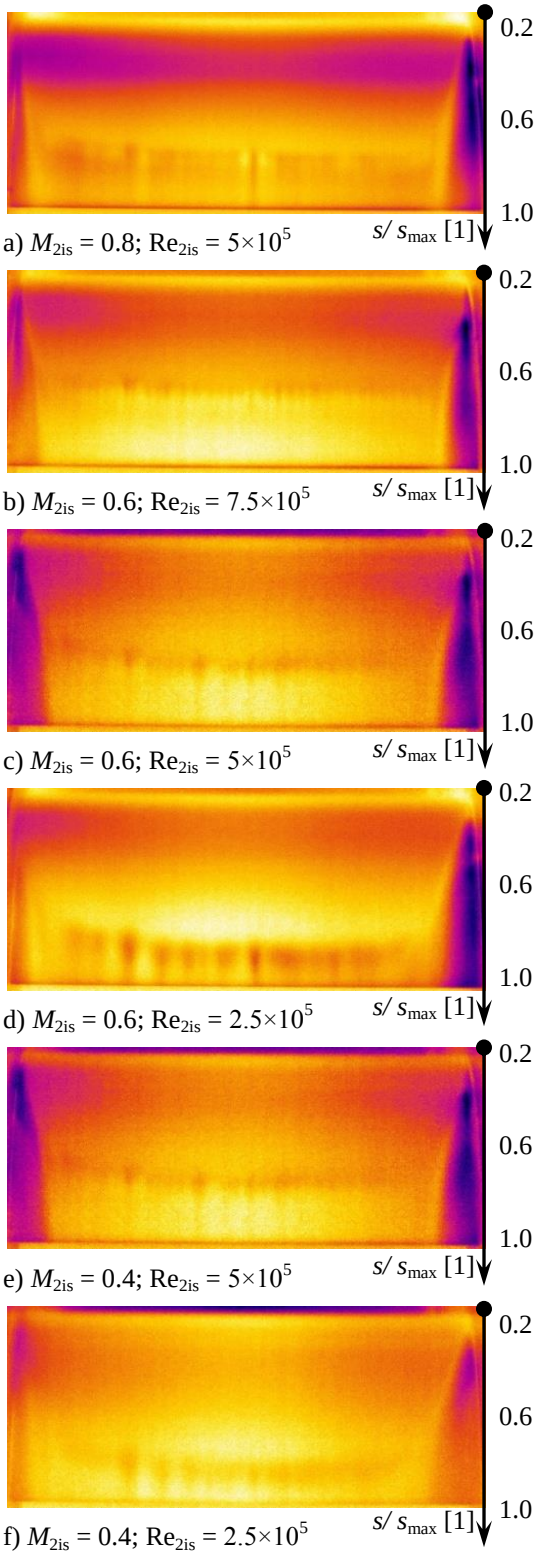

Figure 5: Visualization of the BL transition using IRT.

Structures in the BL transition zones (Figure 5a and c – f), where the blade surface had lower temperature, are visible. These structures were formed by small separation "bubbles" and by longitudinal vortices, which can be connected with the BL transition. In these "bubbles" heat transfer between the free stream and blade surface was decreased. It corresponds with theory of heat transfer in separated flow; see e.g. Baehr and Stephan [23].

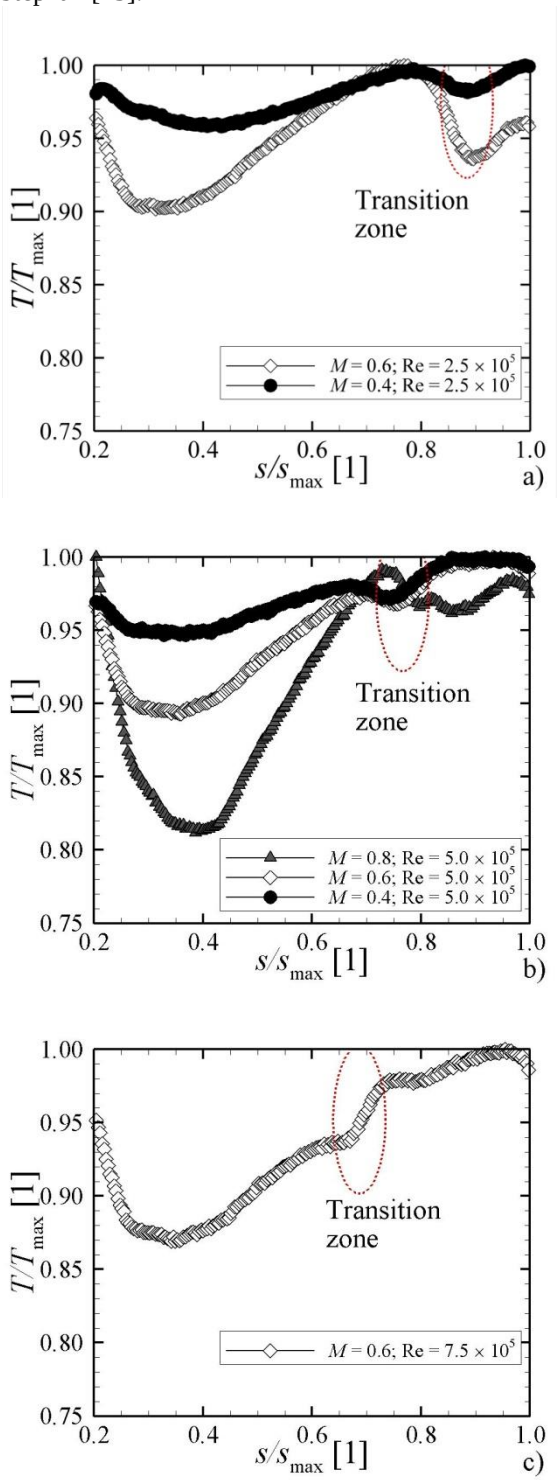

Figure 6: Normalized temperature distributions along the s coordinate of the blade: a) $Re_{2,is}$ = 2.5×10^5, b) $Re_{2,is}$ = 5.0×10^5, c) $Re_{2,is}$ = 7.5×10^5.

In all Figures 5a – f, corner vortices on both sides of the test section can be clearly seen as wedge regions with lower temperature. These vortices are generated as interaction of the inlet BLs on the WT walls and leading edge of the

blade. In these regions enhanced cooling of the blade surface was observed. That was caused by the cooler fluid, which temperature was reduced in the BLs on the WT walls that had lower temperature compared to the free stream and also blade. Cooling effect is caused also as a consequence of the fluid leakage from the pressure side of the blade to the suction side through the gaps between the blade and the WT walls.

Normalized temperature distribution T/T_{max} along the blade coordinate s is shown in Figure 6 (T_{max} is the maximal temperature from the measured profile). Transition of BL on the blade surface is highlighted by doted ellipse in the figures.

Pressure distribution on the blade surface is shown in Figure 7. Ratio of the local static pressure and inlet total pressure is plotted in the figure. Pressure distribution was measured during the work of Kladrubský [24], and only relevant unpublished data are shown here.

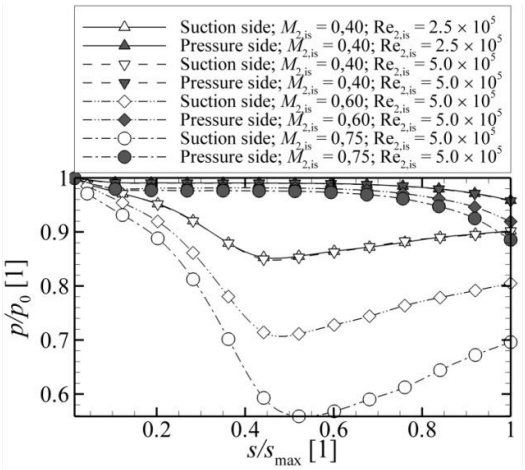

Figure 7: Pressure distributions on the blade surface.

NUMERICAL RESULTS

In Figure 8 field of the intermittency coefficient γ, for 2D simulation using the transition model of Straka and Příhoda [19] in location near the trailing edge, is shown. The intermittency coefficient takes value $\gamma = 0$ in domain of laminar flow (blue color in Figure 8), value $\gamma = 1$ in domain of turbulent flow (red color in Figure 8) and values in range $0 < \gamma < 1$ in transition region. Figure 8 shows the effect of the Reynolds number on the transition onset for case of $M_{2is} = 0.6$.

Figure 9 shows distribution of the pressure coefficient $c_p = (p_{sf} - p_S)/(p_T - p_S)$ along the blade surface for 2D simulation. p_{sf} is the pressure on the blade surface, p_S and p_T are the static and total pressure of the inlet stream. Curvilinear coordinate s has origin at the leading edge, s_{max} is the curvilinear length of the suction or pressure surface respectively.

In Figure 10 there is shown distribution of normalized temperature T_{sf}/T_T along the blade surface for 2D simulation. T_{sf} is the temperature on the blade surface and T_T is the total temperature of the inlet stream.

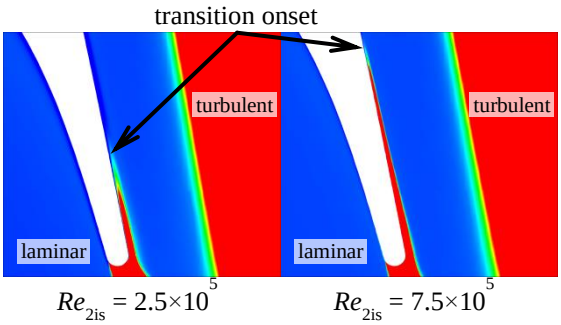

Figure 8: Field of intermittency coefficient γ for 2D simulation; $M_{2is} = 0.6$.

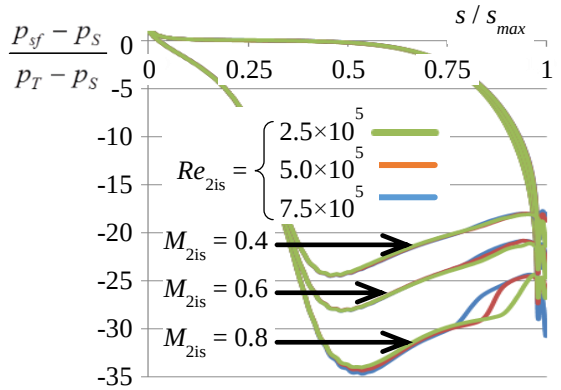

Figure 9: Pressure coefficient distributions along the blade surface for 2D simulation.

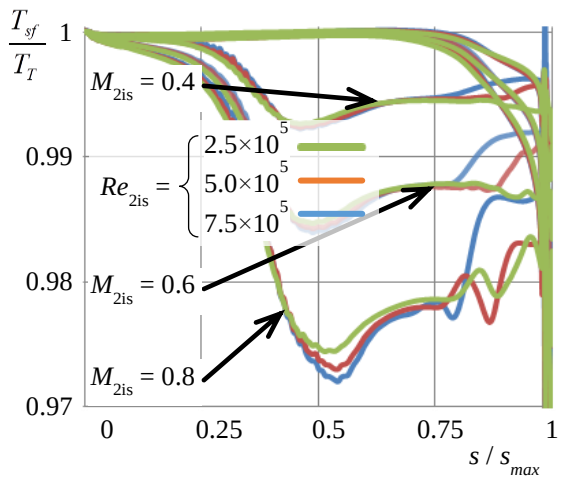

Figure 10: Normalized temperature distributions along the blade surface for 2D simulation.

In Figure 11 the surface temperature on suction side of blade for 3D simulation using transition model of Kubacki and Dick [20] is shown. Direction of view is the same as in Figure 5. Black line shows position of the transition onset. Figure 11 illustrates the effect of the Reynolds number as well as the effect of the side walls on the transition

onset. It should be noted that both the blade surface as well as the side wall are modeled as adiabatic walls without any heat transfer, which is in contrary with reality in test section of the wind-tunnel where the side walls have a cooling effect.

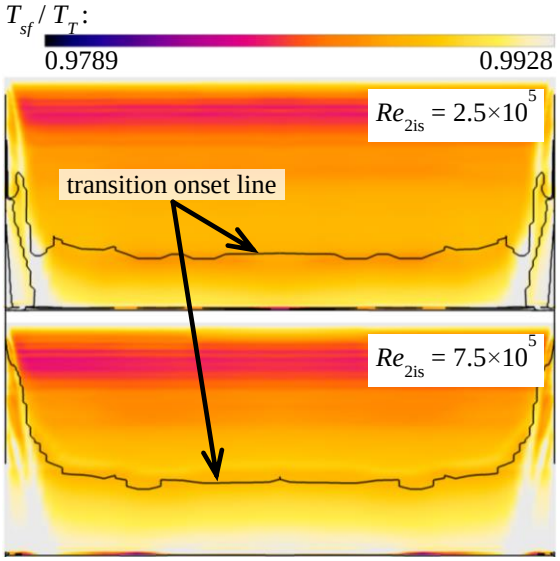

Figure 11: Field of normalized surface temperature for 3D simulation; M_{2is} = 0.6.

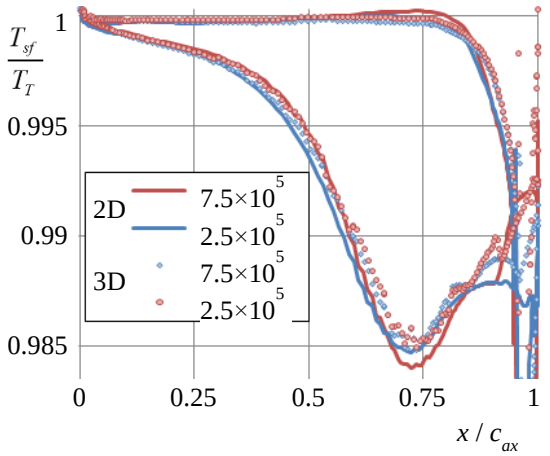

Figure 12: Comparison of normalized surface temperature distribution of 2D and 3D simulation; M_{2is} = 0.6.

Figure 12 shows comparison of the surface temperature distribution along the axial chord for 2D and 3D simulation in the middle of the blade span.

COMPARISON OF THE USED METHODS

Comparison of used methods is based on the evaluations of the positions of the BL transitions made of both approach. These comparisons are listed in Table 2. As can be seen, the CFD prediction is in good agreement with experimental results.

Comparison of dimensionless pressure distribution p/p_0 on the blade surface obtained from pressure measurement and CFD is shown in Figure 13. Good agreement between both used approaches can be seen from the mentioned figure.

Table 2: Position of the BL transition - comparison of used methods.

$M_{2,is}$[1]	$Re_{2,is}$[1]	s/s_{max} [1]	
		IRT	2D CFD
0.4	2.5×10^5	0.80	0.82
	5.0×10^5	0.75	0.78
	7.5×10^5	-	0.74
0.6	2.5×10^5	0.80	0.82
	5.0×10^5	0.75	0.78
	7.5×10^5	0.70	0.74
0.8	2.5×10^5	-	0.82
	5.0×10^5	0.75	0.78
	7.5×10^5	-	0.74

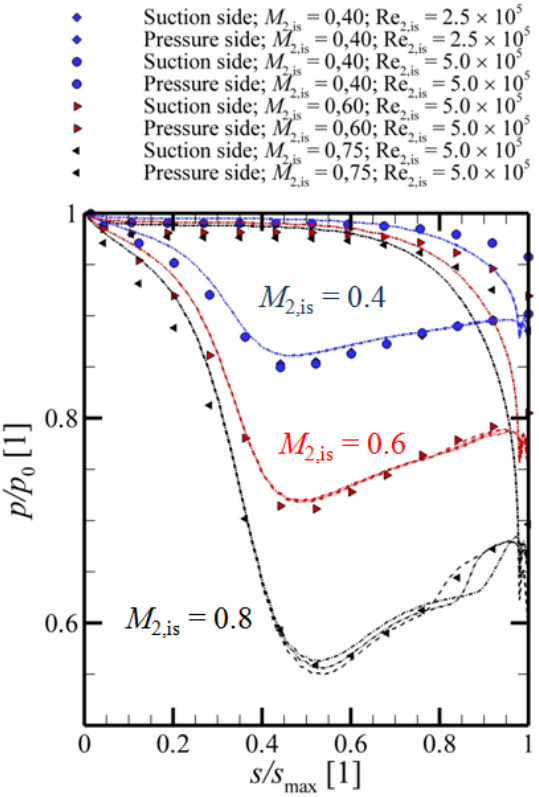

Figure 13: Comparison of normalized surface pressure distribution p/p_0 on the blade surface obtained from experiments and CFD.

CONCLUSION

Experimental and numerical investigation of the BL transition on the prismatic blade in the linear blade cascade was topic of this contribution. For the experimental detection of the BL transition the method of Infrared thermography was used. Numerical calculations were performed by in-house numerical codes based on the finite volume methods. Two different algebraic models of the BL transition were applied during the calculations.

Influences of Reynolds and Mach numbers on the BL transition were studied. With increasing

Reynolds number position of the BL transition moves upstream toward the leading edge of the blade, while no significant influence of the Mach number on the position of BL transition was observed.

Comparison of the temperature distribution on the blade surface (Figures 6, 10 and 12) shows good agreement between the experimental and numerical approach.

The 3D numerical simulation (Figure 11) shows the similar surface temperature distribution as was detected by experiment (Figure 5). The adiabatic side wall condition used in computations gave the only differences in temperature in the side wall vortices.

ACKNOWLEDGMENTS

This project result was developed within the institutional support of the Ministry of Industry and Trade of the CR directed to the development of research organizations.

REFERENCES

[1] Narasimha, R.; 1985. "The laminar-turbulent transition zone in the boundary layer". Prog. Aerospace Sci., Vol. 22

[2] Mayle, R. E.; 1991. "The role of laminar-turbulent transition in gas turbines engines". Journal of Turbomachinery, 113

[3] Gomes, R. A.; Stotz, S.; Blaim, F.; Niehuis, R.; 2015. "Hot-film measurements on a low pressure turbine linear cascade with bypass transition". Journal of Turbomachinery, Vol. 137

[4] Balla, J. V.; 2012. "Pressure-sensitive paint for detection of boundary layer transition". Master's Thesis, Ohio State University

[5] Cattafesta, L. N.; Iyen, V.; Masad, J. A.; King, R. A.; Dagenhert, J. R.; 1995. "Three-dimensional boundary layer transition on a swept wing at Mach 3.5". AIAA Journal, Vol. 33

[6] Astarita, T.; Carlomagno, G. M.; 2013. "Infrared Thermography for Thermo – Fluid – Dynamics". Springer – Verlag

[7] Zuccher, S.; 2017. "Infrared thermography investigations in transitional supersonic boundary layers". Exp. Fluids, Vol. 44, 2007.

[8] Yokokawa, Y.; 2005. "Transition measurement on metallic aircraft model in typical low speed wind tunnel". Trans. Japan Soc. Aero. Space Sci., Vol. 48

[9] Joseph, L. A.; Borgoltz, A.; Devenport, W.; 2016. "Infrared thermography for detection of laminar-turbulent transition in low-speed wind tunnel testing". Exp. Fluids, Vol. 57

[10] De Luca, L.; Carlomagno, G. M.; Buresti, G.; 1990. "Boundary layer diagnostic by means of an infrared scanning radiometer". Exp. Fluids, Vol. 9

[11] Patorski, J. A.; Bauer, G. S.; Theo, J.; 2001. "Two-dimensional and dynamic method of visualization of the flow characteristics in a convection boundary layer using infrared thermography". Journal of Theoretical and Applied Mechanics, Vol 39

[12] Baek, P.; Fuglsang, P.; 2009. "Experimental detection of transition on wind turbine airfoils". Wind energy conference

[13] Raffel, M.; Merz, Ch. B.; Schwermer, T.; Richter, K.; 2015. "Differential infrared thermography for boundary layer transition detection on pitching rotor blade models". Exp. Fluids, Vol. 56

[14] Jelínek, T.; 2017. "Experimental investigation of the boundary layer transition on a laminar airfoil using infrared thermography". Exp. Fluid Mech. conf. proc.

[15] Flídr, E.; Jelínek, T.; 2018. "Experimental investigation of the boundary layer transition on the prismatic blade using infrared thermography". Application of Experimental and Numerical Methods in Fluid Mechanics and Energy, conf. proc.

[16] Michálek, J.; 2016. "Turbine profile P50_Rte0.8". Technical report VZLU R-6541, Prague, (In Czech)

[17] Hellsten, A.; 2004. "New two-equation turbulence model for aerodynamics applications". Ph.D. thesis, Helsinki University of Technology

[18] Straka, P.; 2013. "Calculation of 3D unsteady flow in axial stage of low power experimental turbine". Technical report VZLU R-5904, Prague, (In Czech)

[19] Straka, P.; Příhoda, J.; 2010. „Application of the algebraic bypass-transition model for internal and external flows", Proc. Conf. Exp. Fluid Mech. 2010, Liberec, pp. 636-641

[20] Kubacki, S.; Dick, E.; 2016. "An algebraic model for prediction of bypass and separation-induced transition in turbomachinery boundary layers". Proc. 11th Int. ERCOFTAC Symp. on Engineering Turbulence Modelling and Measurements, Palermo

[21] Walters, D. K.; Cokljat, D.; 2008. "A three-equation eddy-viscosity model for Reynolds-averaged Navier-Stokes simulations of transitional flow". J. Fluids Engineering, Vol. 130, 121401/1-40

[22] Carlomagno, G. M.; Cardone, G.; 2010. "Infrared thermography for convective heat transfer measurements". Exp. Fluids, Vol. 49

[23] Baehr, H. D.; Stephan, K.; 2011. "Heat and Mass transfer". 3th edition, Springer – Verlag Berlin Heidelberg

[24] Kladrubský, M.; 2014. "Blade cascade Leitring". Technical report VZLU R-6253, Prague (In Czech)